Available online at www.sciencedirect.com
SCIENCE DIRECT®
Wear 254 (2003) 635–644
WEAR
www.elsevier.com/locate/wear

Characterization and mechanical modeling of the abrasion properties of sintered tools with embedded hard particles

M. Borri-Brunetto, A. Carpinteri, S. Invernizzi*

Department of Structural and Geotechnical Engineering, Corso Duca degli Abruzzi 24, Politecnico di Torino, Torino, Italy

Received 12 April 2002; accepted 10 March 2003

Abstract

A wide variety of applications, ranging from rough cutting of stone and concrete to ultra-precision machining of ceramics for electronic components, are commonly performed with the so-called super-abrasive tools. The working part of such tools is made of hard particles, typically diamonds or cubic boron nitride crystals, embedded in a resin or sintered metal matrix. The performance of the tool is influenced by many technological aspects, but basically depends on the abrasion property of the hard particles-matrix system.

In the present paper, a mechanical approach is followed in order to link the performance of a tool to some relevant design parameters, i.e. hard particle content and diameter. The model is based both on theoretical and experimental evidences.

An experimental technique is described for the tool characterization, based on a coupled optical and laser-scanner acquisition of the tool working-surface. Moreover, the tool design parameters are put into play through a stereological model. The numerical strategy of the presented model is justified by a preliminary study of the contact stress distribution over the contact area.

Different useful parameters (i.e. distribution of contact stresses, number of active particles, etc.) are obtained from the numerical simulation of abrasion, although the performance of the tool is primarily evaluated from the estimated removed volume.

Keywords: Abrasion; Plowing; Cutting; Super-abrasives

1. Introduction

The mechanics of cutting and shaping processes performed by super-abrasive tools [1] can be ascribed mainly to abrasion phenomena. Actually, the local behavior of each hard particle depends on many variable parameters. The local contact force is responsible both for the indentation depth and for the tangential reaction. Furthermore, depending on the base material, the volume removal can be due to the plastic flow in metals [2], as well as to chips formation in ceramic-like brittle materials [3].

Usually the process is performed in lubricated conditions, where the circulating fluid has both the goals of cooling the tool and, if necessary, to evacuate the chips minimizing the energy consumption due to the unavoidable milling processes. The shape of the tool is another important aspect of the problem, but the present approach is largely independent of the particular application.

The matrix (i.e. the bonding system) also plays a very important role, as it is responsible of retaining the rigid inclusions against pull-out mechanisms. On the other hand, the wear properties of the metal matrix should be tuned in order to control the rate at which new hard particles emerge as the older ones become blunt and lose their cutting capability [4].

The mechanical properties of hard particles themselves are relevant. In fact, hardness and fracture energy are the principal factors that influence the durability as well as the re-sharpening of damaged particles [5].

During the machining or cutting process, many particles interact with the base material in a complex manner so that their collective behavior cannot be simply obtained as a summation of the effects of each single particle. In particular, the protrusion of the rigid particles from the matrix accounts for the actual distribution of local forces. For example, a nonlinear thrust-penetration law for the tool can be obtained from a linear indenter behavior in the case of nonuniform protrusion of hard particles from the matrix. Thus, an exact picture of the tool profile must be drawn prior to any numerical simulation.

In the following section, an experimental technique to characterize the exact topography of the tool is presented, coupling classical image analysis with a laser-scanner acquisition of the surface profile [6]. This allows a determination of the horizontal position of all hard particles as well as of

* Corresponding author. Tel.: +39-011-564-4860; fax: +39-011-564-4899.
E-mail address: stefano.invernizzi@polito.it (S. Invernizzi).

0043-1648/03/$ – see front matter © 2003 Elsevier Science B.V. All rights reserved.
doi:10.1016/S0043-1648(03)00254-0

their protrusion, which will be related to the distribution of the total thrust among the particles.

An objective characterization of the tool surface should rely on statistical concepts. Moreover, it is useful to link the tool profile characteristics with some relevant design data (i.e. size and shape distribution of the particles). Therefore, a simple stereological model is proposed, which links the main geometrical parameters of the hard particle distribution (radius of particles, volume concentration) to their relative protrusion from the sintered matrix.

The abrasion properties of the tool are deeply influenced by the distribution of stress between the tool and the base material. Different cases are taken into consideration through numerical simulation of contact, ranging from the linear-elastic normal interaction to the rigid-perfectly plastic case. The two limit cases result to be rather similar, as could not be guessed at first sight, because in both cases only a few hard particles are in contact with the base material, under realistic load conditions.

The extremely localized patterns obtained from the contact simulations suggested to proceed with a coarse-grained approach, and to consider the size of particles as the relevant scale length. The mechanical behavior of an isolated particle can be evaluated from single-scratch experimental tests [7] as well as from numerical lattice simulation [8]. As a result of the numerical abrasion simulation of a multi-particle tool, different physical quantities can be obtained, like the number of active particles, the distribution of contact forces and an estimate of the removed volume.

Finally, it is worth noting that an optimization of the tool design could be attained by generating, with a numerical procedure, tool surfaces with the required statistical properties. The parameters of the particle distributions could then be adjusted in order to maximize the efficiency of the tool in terms of volume removal.

2. Geometrical characterization of the tool surface

The active surface of the tool shows a spatial as well as a temporal variability. The former is due to the statistical dispersion of particles in the matrix. The latter is caused by particle renewal, with fracture and pull-out of old particles and emerging of new ones from the worn matrix. Thus, each snapshot of the surface can be considered, from a statistical viewpoint, as a sample of the population of active surfaces.

The acquisition of in-plane position and height of the particles emerging from the sintered matrix is not a simple task, and cannot be achieved in a single step [9]. Therefore, it is useful to couple two techniques, namely optical scanner imaging and laser measurements of surface topography. In addition, a stereological model is presented that is able to link the information acquired (i.e. heights profile, number of emerging particles, etc.) with some relevant design parameters of the tool (e.g. particle fraction and diameter).

2.1. Experimental acquisition

Some basic geometrical information, like the number of particles protruding from the matrix and their relative in-plane position, can be easily recovered from the image analysis of the tool.

Classical photography presents some disadvantages, mainly due to variable illumination conditions and optical distortions. Better results can be obtained by digital acquisition of the image, positioning the tool directly on the glass of an optical scanner, so that the same uniform illumination conditions are provided at each acquisition. Moreover, the acquisition resolution can be easily tuned and it is possible to assess, without any re-scaling, the horizontal position and apparent diameter (size of the emerging portion) of the particles.

The hard particles are easily recognizable, thanks to their color, different from the metal matrix (Fig. 1a). For better contrast, the tool surface has been wetted. It is worth noting that, in this case, a 1200 DPI scanner is largely enough to estimate the in-plane position of each emerging hard particle and their number, the resolution being approximately 20 μm and the mean particle diameter in the range 200–400 μm.

The relative protrusion of the hard particle from the matrix is crucial in the study of the contact interaction between tool and base material. Therefore, an innovative experimental methodology has been developed to digitize the three-dimensional topography of surfaces at the meso-scale. The surface height measurements are performed by means of a laser apparatus, counting the number of wave-cycles between the ray emission and the ray reception after the reflection on the specimen surface. The specimen to be analyzed is fixed, whereas the horizontal position of the laser is controlled by two orthogonal micrometric step-motors. A PC controls the motors and provides the analogic-digital conversion of the laser signal. Especially developed software provides extreme versatility and the full automation of the surface acquisition process. The digitized surfaces can extend over a 50 mm × 100 mm area, and a 2 μm maximum accuracy can be achieved, both in vertical and horizontal direction. An overflow signal is obtained when the laser ray is reflected away in an anomalous manner, but only a few overflows have been detected for each acquisition. The height of such points has to be interpolated between neighbors. In order to compare the results from different acquisitions, each data set has been de-trended, referring each height field to the surface mean plane, calculated with a mean-squares algorithm.

It is useful to adopt the same resolution for both the image and the surface height acquisitions (30 mm in the present case). In this way, a plane rotation and translation transformation provides a good matching of the two data sets.

Data related to segments of a core-bit after 225 cm of perforation in concrete are used in this paper as an example of the applied methodology. In Fig. 1b, the contour plot of

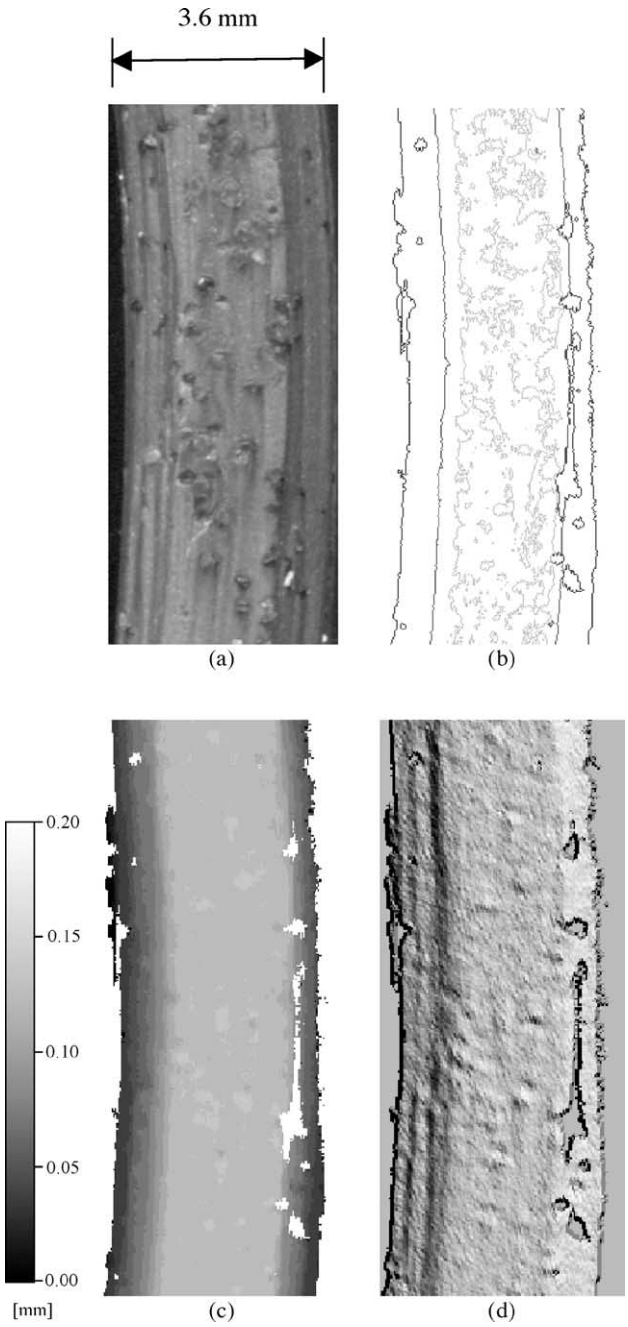

Fig. 1. Tool surface: scanner image (a); height contours (b); gray scale plot (c); shaded relief (d).

the tool surface is shown, whereas in Fig. 1c surface heights are depicted as a gray-level image. Fig. 1d is obtained by means of a shadowing algorithm applied to the height field data.

The heterogeneity of the tool bulk (particles dispersed in the matrix) reflects in the characteristics of the tool surface. Therefore, the profile is not smooth, and it is possible to discriminate between the small-scale roughness of the matrix, and the larger scale roughness due to the emerging particles. The two length scales are well separated, unlike the case of rough surfaces obtained from fracture of concrete or rock [10], where all the scales come into play. Consequently, no fractality is detected analyzing the profile.

The measured tool profile is used in the following to determine the contact stress distribution with a detail given by the resolution adopted in the acquisition. On the other hand, the plowing simulation mainly concerns the scale of the particles. The in-plane position of each hard particle is provided by the image analysis. The protrusion of the particle is obtained by reading the height of the laser-scanned profile at the same location.

2.2. Statistical model

Based on some assumptions about the average shape and size of the particles, a simple stereological model can be used to link the information provided by the experimental acquisition of the tool geometry to some more relevant design parameters of the super-abrasive tool, i.e. size, density and shape of the particles.

During the working life of the tool, both matrix and particles are progressively damaged. The metal is abraded by the action of chips detached from the base material, which is harder than the metal. Particles tips are broken if, during the process, their exposed portion exceeds a threshold.

In the following, we will call protrusion of the particles, above the mean surface of the sintered matrix, the height that a hard particle can reach before it is broken or pulled out from the matrix.

Given the volumetric density c of particles per unit volume of the matrix, and the equivalent diameter d of a particle, as defined in Fig. 2a, the number of particles per unit volume is

$$n = \frac{c}{Md^3}, \tag{1}$$

where M is a nondimensional coefficient that depends on the shape of the particle as shown in Table 1. The diameter d is assumed to be a constant for a given tool.

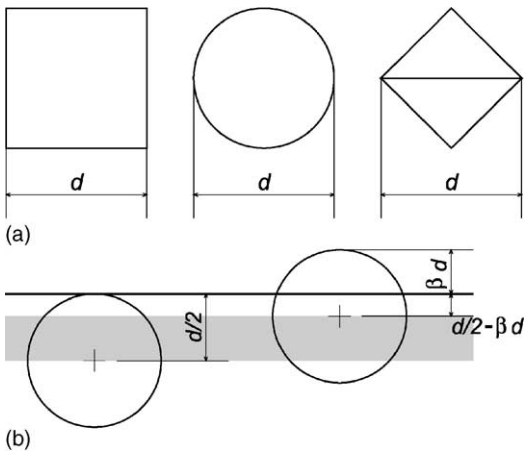

Fig. 2. Definition of the diameter of a hard particle (a); reference volume for calculating the number of exposed hard particles (b).

Table 1
Shape factor M for different shapes of a particle

	M
Cube	1.00
Sphere	0.52
Octahedron	0.33

At any stage of the working life of the tool, after an initial transient condition, the number of exposed particles on a surface of area A can be estimated by considering the number of particles whose centroids are included in a reference volume (Fig. 2b):

$$V = A\left[\frac{d}{2} - \left(\frac{d}{2} - \beta d\right)\right] = \beta A d, \tag{2}$$

where β is the maximum fraction of particle size that can project above the base metal without breaking, e.g. if $\beta = 1/3$, the particle will break when its height above the matrix surface will reach one-third of its diameter.

The number of visible particles is given by

$$N = nV = \left(\frac{c}{Md^3}\right)\beta A d = \frac{\beta c}{M}\left(\frac{A}{d^2}\right), \tag{3}$$

so that the relative protrusion can be expressed as

$$\beta = \frac{MNd^2}{Ac}. \tag{4}$$

By fixing the volumic content c, given the density N/A of observed emerging particles, the relative protrusion can be evaluated and plotted vs. the diameter d, as shown in Fig. 3.

It is worth noting that the assumption of homogeneous spatial distribution of particles in the volume corresponds to a linear distribution of heights among the emerging particles [11]. From a practical point of view, Eq. (4) links the number of emerging particles (observed parameter) with the particle volumic content (design parameter) and the particle protrusion (observed parameter). Finally, the present simple model could be used to generate synthetic tool profiles, useful to further optimization studies of any tool design factor (e.g. the hard particle content).

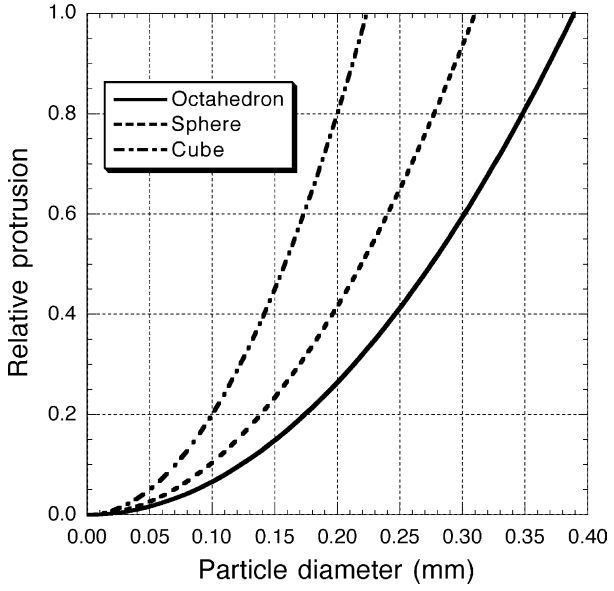

Fig. 3. Relative protrusion β as a function of the diameter of the hard particles d for different shapes. Volumic content $c = 7\%$, surface density of particles $N/A = 1.4\,\text{mm}^{-2}$.

3. Numerical simulation of contact

The cutting capability of each hard particle depends on its local contact pressure against the base material as well as its shape. Moreover, contact stresses are responsible for the wear of both the particles and the matrix. Mechanisms as flattening or re-sharpening of hard particles have a strong influence on tool performance, while the matrix should have an optimal consumption rate, in order to release blunt particles and allow the growth of new ones.

The mechanical behavior of a single indenter can be simulated numerically with great detail [8], although, due to the great computational effort required, this approach could not be pursued to study the entire tool. On the other hand, it is possible to calculate the stress field developed by contact between the tool and the base material including all the interesting details of the surface [12]. This computation has been performed under different constitutive hypotheses: either linear-elastic or rigid-perfectly plastic behavior. The aim of the analysis is to give an idea of the distribution of contact forces exchanged between the matrix and the population of emerging particles. Obviously, linear elasticity and perfect plasticity are two limit cases, while the actual situation is comprised in between.

3.1. Linear-elastic normal interaction

In order to evaluate the distribution of contact forces between tool and base material, as a first approximation a simply orthogonal, linear-elastic numerical model has been used.

The solution of the unilateral problem is searched by means of a numerical technique particularly well suited to take into account the finest details of the contacting surfaces.

The numerical procedure is designed in order to determine the geometrical properties of the contact domain between the half-spaces, which is initially unknown. The solution of the problem can be conveniently achieved by means of an incremental-iterative algorithm (*active set strategy*). The resolution adopted in solving the problem corresponds to the experimental resolution (30 μm). In the following, we call "contact point" the elementary spot with 30 μm diameter.

As the code can simulate the presence of only two materials, without discriminating between the different mechanical properties of hard particles and metal matrix, two different cases have been considered:

- a *stiff* situation, in which the segment has been given a virtually infinite Young's modulus ($E_{base} = 36\,GPa$, $E_{segm} = 10^4 E_{base}$);
- a *soft* situation, where both the contacting bodies are made of the same concrete-like base material ($E_{base} = E_{segm} = 36\,GPa$).

The evolution of the contact domain has been followed up to a very high load, namely nearly 10 kN, corresponding to a mean nominal pressure of about 200 MPa. It should be noted that this is an extremely high load with respect to real conditions.

The numerical model adopted here calculates the response of the interface at a given value of imposed relative displacement between distant points of the contacting bodies. For brevity, in the following, this parameter will be called *penetration*.

The load–penetration curves are reported in Fig. 4, together with the number of contact points. The calculated contact domains at four levels of the applied load (points A–D in Fig. 4) are shown in Fig. 5((A)–(D)).

The first contact domain (Fig. 5(A)) is referred to a load of about 80 N which could be considered the right order of magnitude of loading in realistic operative conditions. The corresponding real contact area is approximately 0.08% of the nominal contact area.

In the case of soft contact, the only difference with the previous case is the Young's modulus of the segment. In this simulation, the parameter has been chosen equal to the modulus of concrete (contact of two bodies with the same elastic characteristics), so that, in order to obtain the same value of the penetration u, the applied force has to be one-half of that in the stiff case. The number of contact points and the shape of the contact domains depend only on the imposed penetration u, and the results presented previously (Fig. 5) are valid also for the soft contact case at the same penetration.

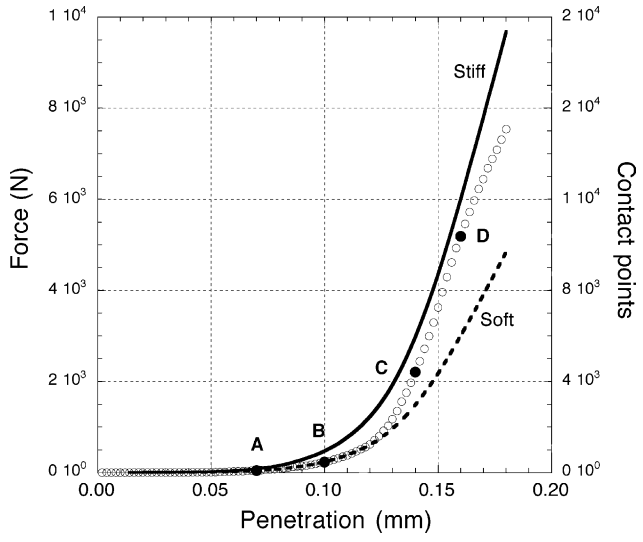

Fig. 4. Load–penetration curves and number of contact points for a segment vs. concrete interface. Points A–D refer to the contact domains shown in Fig. 5. The number of contact points, plotted with open circles, is the same in both cases, depending only on the penetration.

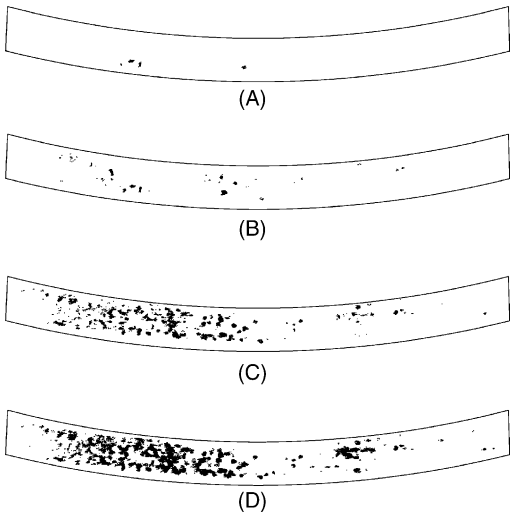

Fig. 5. Sequence of contact domains at increasing penetration (letters A–D refer to points in Fig. 4).

The relation between the applied force and the number of contact points is shown in Fig. 6. Nearly 100 points result in contact at a load of 80 N, although these points, at the considered resolution (30 μm) represent only four larger clusters of contact; each one could be generated by a relatively large single asperity, possibly associated to a hard particle, as can be seen in Fig. 5(A).

3.2. Rigid-perfectly plastic orthogonal interaction

Another approach to the meso-scale description of the geometrical and mechanical nonlinear contact interaction

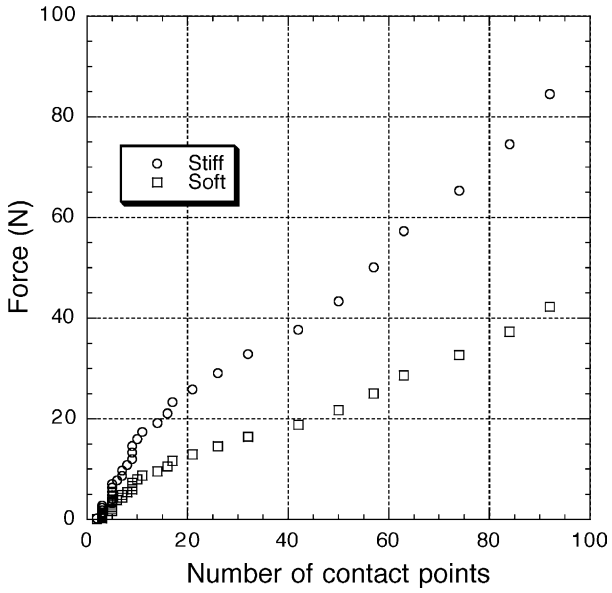

Fig. 6. Number of contact points for stiff and soft cases.

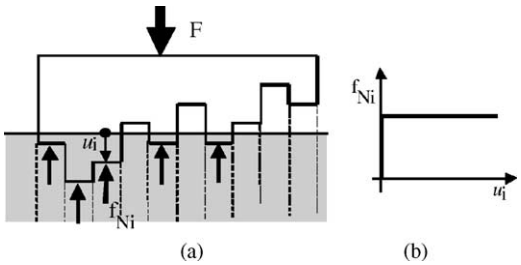

Fig. 7. Scheme of the rigid–plastic interaction (a); base material constitutive law (b).

between the tool and the base material is the rigid-perfectly plastic assumption.

Following this hypothesis, the same core-bit segment analyzed in the previous section is assumed to be perfectly rigid and with an infinite strength, the concrete base material is modeled as rigid-perfectly plastic, with a finite yielding strength. The interaction between the two bodies is to be considered strictly local, as any contacting point behaves independently of the neighboring ones.

Following this scheme, the surface of the core-bit segment is obtained from the laser acquisition, while the base material surface is assumed to be flat. This assumption allows one to obtain the contact domain related to a certain penetration depth as a particular contour level of the de-trended segment surface.

In this model (Fig. 7a), the total applied load F is the sum of the n micro-forces f_i, transmitted by the n points of contact. Although each contact point is modeled by a simple constitutive law (Fig. 7b), the overall model behavior should result to be realistic, due to the detailed description of the segment topography.

In Fig. 8, the contact domains are shown at increasing penetration depth u: while in the first stage of penetration only very few hard particles are in contact (like in the elastic case), the number of contact points increases with penetration at a faster rate.

The number of the contact points is directly proportional to the total transmitted force, being the ratio equal to the local yield strength f_i. Therefore, it is meaningful to plot the number of contacts vs. the penetration, as shown in Fig. 9.

3.3. Interpretation of the results

The two numerical simulations, regardless to their differences in the constitutive hypotheses, share some common features. Two stages can be recognized considering contact interaction between the tool rough surface and the base material. During an early stage, the contact pattern is highly localized and clustered. This means that only few hard particles (the highest with respect to the mean plane of the surface) are in contact. The total thrust depends not only on the local behavior of each particle, but also on the number of particles that get progressively in contact. In other words,

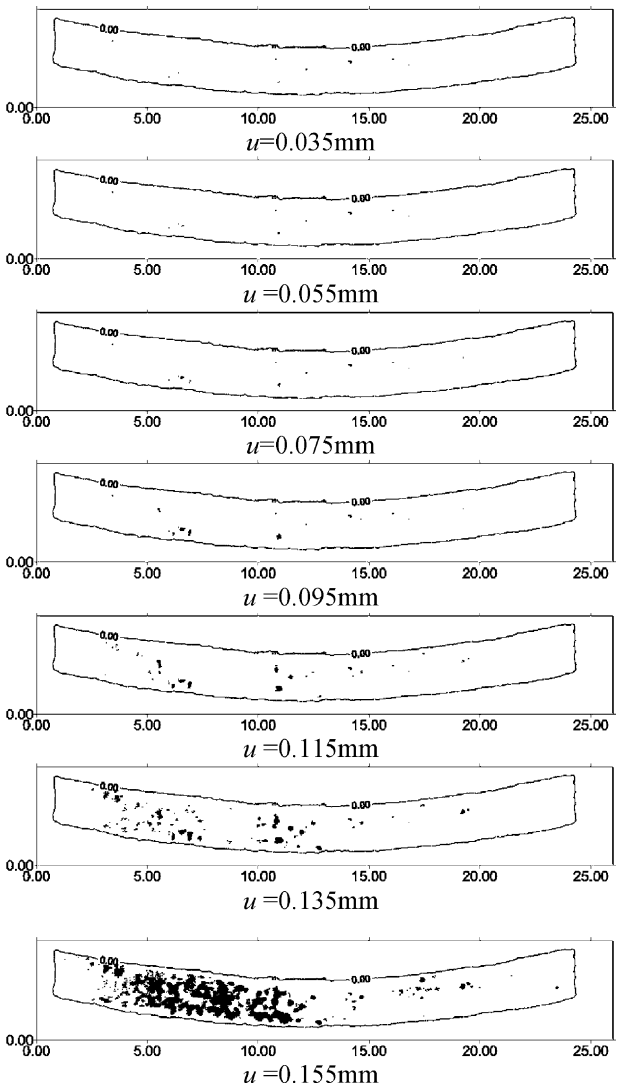

Fig. 8. Contact domain evolution of a core-bit segment at increasing penetration u (plastic interaction model).

the height distribution of the highest particles is the main responsible for the nonlinear thrust-penetration relation.

The later stage could be addressed as a *saturation* regime, where the contact domain increases rapidly (the matrix gets in contact as well) and the total thrust diverges.

Results from elastic as well as plastic simulations are in complete agreement in the range of practical interest (see the comparison in Fig. 10). Under reasonable thrust force (and penetration up to, say, 0.1 mm) only few particles are in contact. It is thus convenient, from a computational and practical point of view, to coarsen the problem, and to consider only the set of the highest particles, instead of the whole tool surface. This procedure will be adopted in the simulation of abrasion presented in the following section.

The numerical results suggest also that the matrix wear is basically due to the milling effect of the removed chips, before they are evacuated by the cooling fluid, rather than to

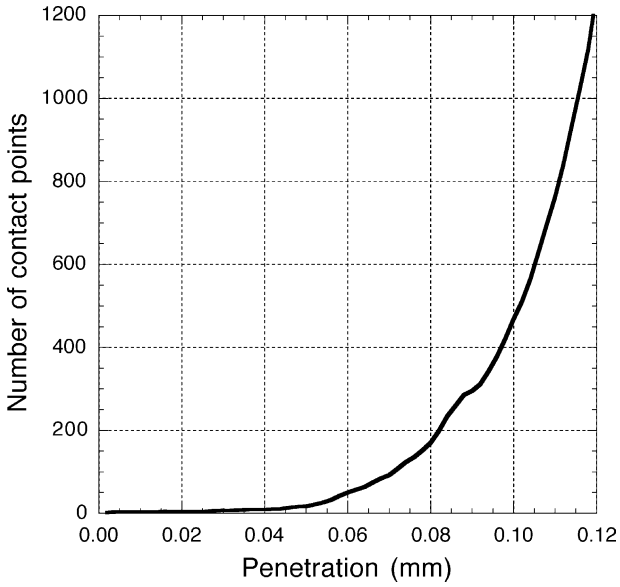

Fig. 9. Number of contact points at 0.02 mm resolution according to the plastic model.

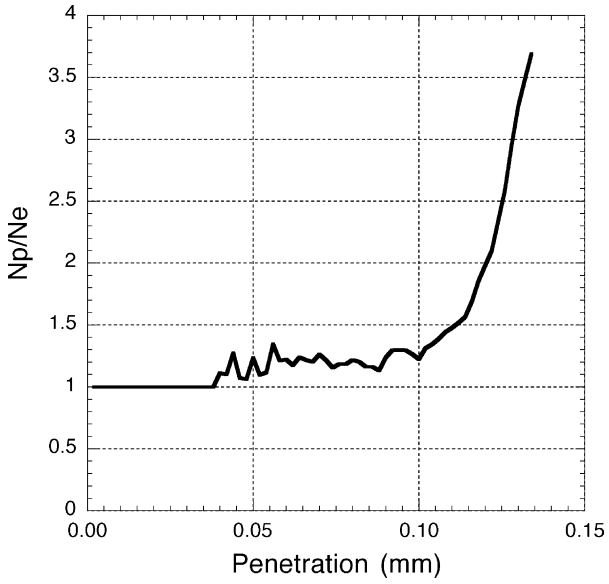

Fig. 10. Ratio of the number of contact points N_p evaluated with the plastic model, to the number N_e of contact points calculated according to the elastic model.

the contact between the matrix and the base material, which would be possible only for extremely high loads.

4. Numerical simulation of abrasion

According to the conclusions from the previous section, the abrasion properties of super-abrasive tools can be simulated numerically taking into consideration only the interaction between the distribution of emerging particles and the base material surface, disregarding the other details of the tool surface.

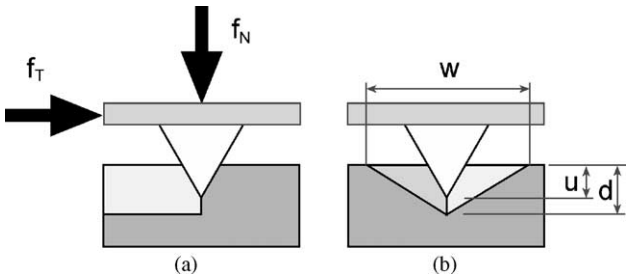

Fig. 11. Scheme of the single-scratch test (a); width and depth of the scratch, resulting from the imposed penetration u (b).

Although both the normal and tangential quasi-static behavior of an indenter acting on a half-space can be obtained numerically [8], dynamical aspects involved in the grooving phenomenon are much more complex to be represented. Therefore, the following model is mainly based on the experimental results obtained from the *single-scratch test*.

4.1. The single-scratch test

The single-scratch test is a well-known experimental procedure to evaluate the hardness of surfaces and coatings (see, e.g. [13]).

The experimental set up, outlined in Fig. 11a, allows to analyze the grooving produced by an indenter scratching a surface. Both normal and tangential forces are acquired during the test, whereas the vertical displacement u is imposed. The diagram representing the data used in the following simulations is shown in Fig. 12. The *post-mortem*

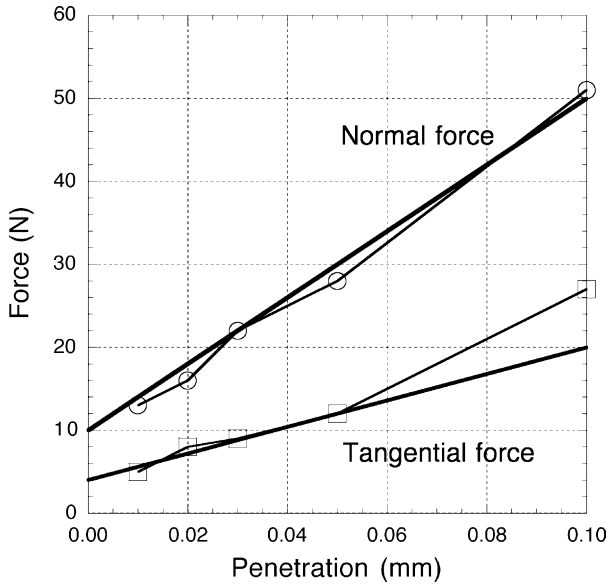

Fig. 12. Forces measured as a function of the penetration depth during a scratch test on the base material.

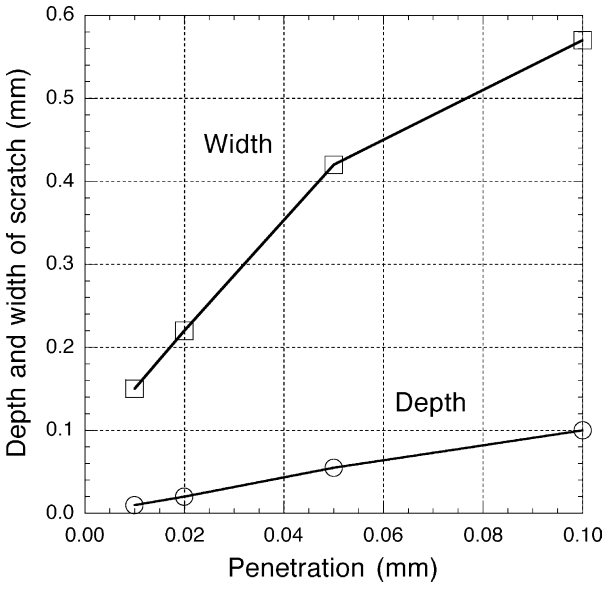

Fig. 13. Width and depth of the groove obtained from a single-scratch test on the base material.

analysis of the surface allows determining the width and the depth of the scratch for increasing penetration (Fig. 13). The cross-section of the groove, schematized in Fig. 11b, can be approximated by a triangle, in order to estimate the removed volume. The real shape of the groove depends on the shape of the indenter. In order to obtain reliable results, to be used in the following plowing model, an indenter similar to the tool particles has been used in the tests.

4.2. The plowing model

The basic task of the model is to evaluate the behavior of a tool as a result of the plowing action of many hard particles. To obtain this result, a few assumptions have to be made:

- negligible interaction between particles (no shadowing or enhancement effects are considered);
- negligible deformation of the tool matrix and of the particles;
- no contact between tool matrix and the base material.

A given penetration u is imposed to the grooving hard particle set, and the forces f_N and f_T, in the normal and tangential direction, required to sustain the process are evaluated. In this context, the normal force f_N no longer represents a simply orthogonal interaction, as in the previous simulations, but should be intended as the normal component arising when a groove is produced by an imposed penetration u.

The results presented in Fig. 12, concerning the single-scratch test on concrete, can be approximated by the linear relation $f_N = 10 + 400u$, where f_N is expressed in N and u in mm (see the upper straight line plotted in the graph). To this force must be associated the tangential micro-force, whose value can be approximated by $f_T = 0.4 f_N$.

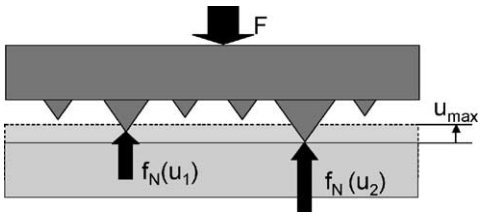

Fig. 14. Scheme of the collective behavior of many hard particles within the same segment.

If the segment, made by metal matrix and hard particles, is considered rigid, the penetration of the highest particle u_{max} can be used as the governing kinematical parameter (Fig. 14). By summing up all the local forces, or micro-forces, $f_N(u_i)$, the total force F on the segment can be calculated as a function of the maximum penetration u_{max}:

$$F = \sum_{i=1}^{N} f_N(u_i), \quad \text{with} \quad u_i = u_{max} - (h_{max} - h_i), \qquad (5)$$

where h_i and h_{max} are, respectively, the heights of the particle i and of the highest particle above a common reference plane.

The response of a single hard particle can be evaluated by modeling each contact as a nonlinear spring with a constitutive law that reproduces the behavior observed experimentally. This phenomenological law is intended only to evaluate the normal micro-force needed to maintain the required penetration during plowing conditions.

The results of the simulations show that the force on a segment required to achieve a penetration of about 100 μm is in the range 1–3 kN. The load on a segment in realistic conditions would presumably be of the order of 0.1–0.5 kN. In the correct working range, the load–penetration curves can be approximated with a power-law, with an exponent larger than one. Therefore, only under very high loads the behavior will tend to be linear.

The calculated force, acting on the entire segment, is shown as a function of the penetration in Fig. 15 for simulations performed on three bit segments of a core-bit, whose geometry has been acquired after 225 cm of drilling. We recall that this result should be interpreted as the thrust on a segment required to obtain a given penetration.

The number of active particles is reported in Fig. 16 as a function of the load. The shapes of the curves show that the number of hard particles in plowing conditions tends to a plateau, corresponding to the saturation condition, where almost all the particles are in contact. If the attention is focused on the first part of the plot, in the realistic loading range, the curves show an almost linear behavior, as reported also in Fig. 17. In addition, the number of grooving particles is small, ranging from 10 to 20, depending on the geometry, at a load of, say, 200 N. By expressing the linear relationship between the load F on the segment and the number N of active particles as

$$N = \kappa F, \qquad (6)$$

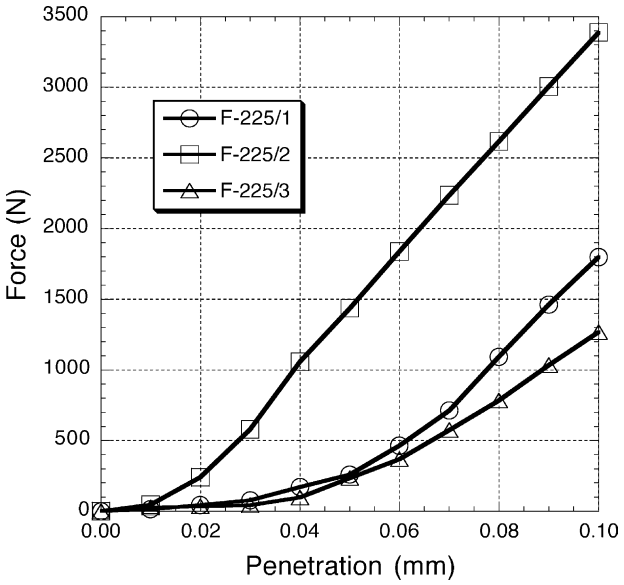

Fig. 15. Normal force vs. penetration on a segment during plowing, for three bit segments of a core-bit, calculated with the plowing model.

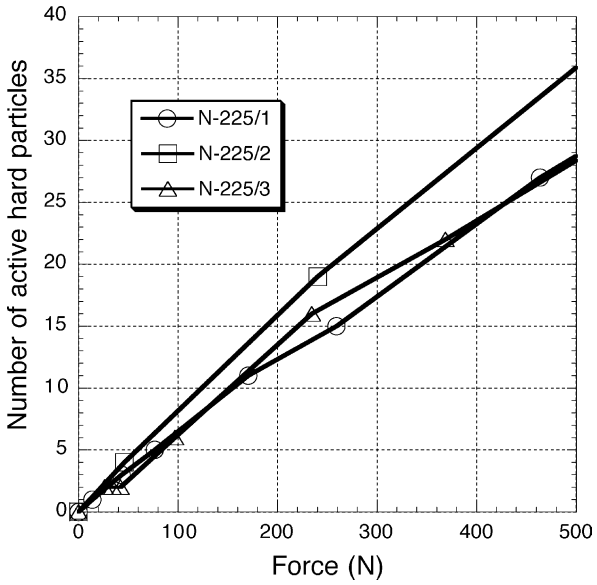

Fig. 17. Detail of the relation between normal force on a segment and number of active hard particles (plowing model).

a reasonable estimate of the proportionality constant based on the simulations is $\kappa \approx 0.07\,\mathrm{N}^{-1}$.

The population of micro-forces on a segment is characterized by its mean value f_{mean}, reported as a function of the load in Fig. 18. It should be remembered that the minimum force needed to initiate penetration in the concrete is equal about to 10 N, following the experimental evidence (Fig. 12). By using the linear approximation of Eq. (6), the estimated value for the mean force is

$$f_{\mathrm{mean}} = \frac{F}{N} = \frac{1}{\kappa} \approx 14\,\mathrm{N}, \tag{7}$$

which is in good agreement with the results of the numerical simulations, as can be seen in Fig. 18.

The diagram in Fig. 19 shows the volume removed per revolution by a segment (the core-bit is composed of nine segments). The volume is calculated as the summation over the set of particles in contact with the substrate, by using the data of Fig. 13. It is worth noting that the removed volume increases, as a function of the thrust, more than linearly. The removed volume is a parameter that estimates quantitatively the performance of the tool.

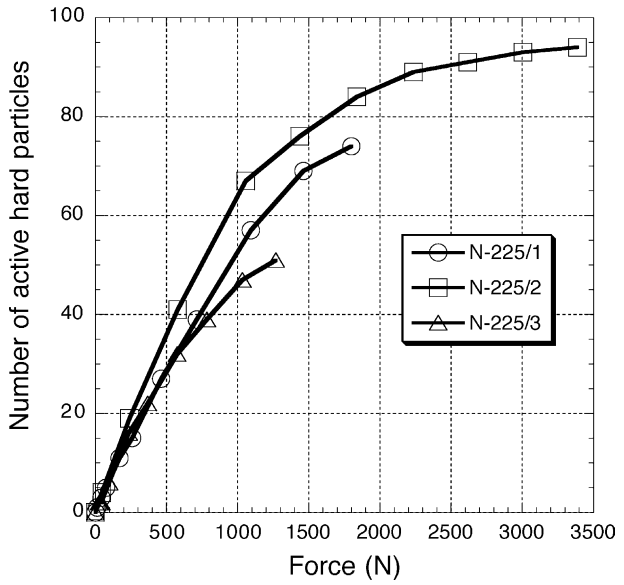

Fig. 16. Number of active hard particles, during plowing, as a function of the normal force on a segment, calculated with the plowing model.

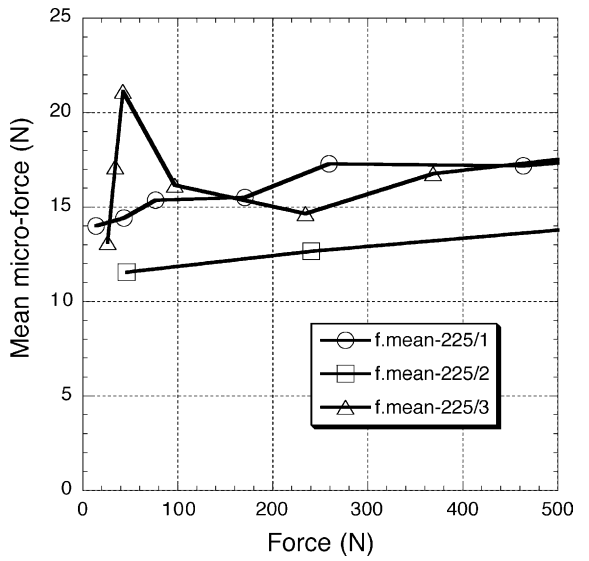

Fig. 18. Mean value of the forces acting on the hard particles vs. normal force, calculated with the plowing model.

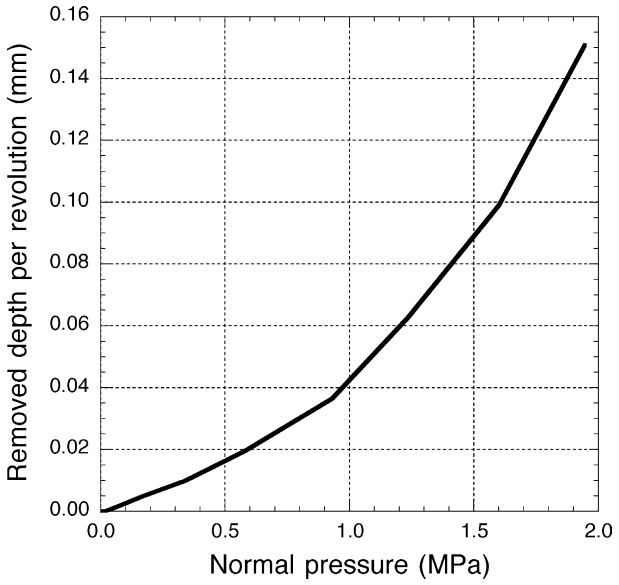

Fig. 19. Estimated removed depth per revolution as a function of the nominal normal pressure acting on the segment.

5. Conclusions

The general approach described is intended to characterize the abrasion properties of super-abrasive tools. The procedure is based on experimental, theoretical and numerical evidences.

The experimental procedure provides an accurate description of the tool surface, by coupling image analysis and laser acquisition of the tool geometry. The experimental information is linked to relevant design parameters with the introduction of a simple stereological model.

A preliminary study of the contact interaction between tool and base material allows determining the distribution of contact forces. It is thus possible to conclude that, under a reasonable thrust, only the hard particles emerging from the matrix get in contact. Therefore, it can be concluded that the wear of the matrix is mainly due to the milling process of the removed chips.

Since the abrasion of the tool depends on the set of particles in contact, the whole mechanism can be studied as the summation of the grooving of each particle. In this way an abrasion model is derived, whereas the nonlinear mechanical behavior of the single particle is introduced experimentally on the basis of single-scratch tests.

The model is able to reproduce various aspects of the problem. Some of them, like the contact force distribution and the number of active particles, are of mechanical relevance. On the other hand, the performance of the tool can be assessed, from a technological point of view, considering the removed volume and therefore the demolition ability.

Acknowledgements

The authors gratefully acknowledge support by the Italian Ministry of Education, University and Research (MIUR) under grant COFIN 2000: *Contact Mechanics: Constitutive laws for interface phenomena and discretization techniques*.

References

[1] K. Subramanian, Superabrasives, in: J.R. Davis (Ed.), Metals Handbook, 9th ed., vol. 16, Machining, ASM, Metals Park, OH, 1989.
[2] H. Ernst, Physics of metal cutting, Machining of Metals, American Society for Metals, 1938, pp. 1–34.
[3] A.W. Ruff, A.W. Shin, C.J. Evans, Damage processes in ceramics resulting from diamond tool indentation and scratching in various environments, Wear 181 (1995) 551–562.
[4] S.F. Krar, E. Ratterman, Superabrasives: Grinding and Machining with CBN and Diamond, McGraw-Hill, New York, 1990, pp. 140–151.
[5] D. Miller, A. Ball, The wear of diamonds in impregnated diamond bit drilling, Wear 141 (1991) 311–320.
[6] A. Carpinteri, B. Chiaia, S. Invernizzi, Three-dimensional fractal analysis of concrete fracture at the meso-level, Theoret. Appl. Fract. Mech. 31 (1999) 163–172.
[7] A. Broese van Groenou, N. Mann, J.B.D. Veldkamp, Single-point scratches as a basis for understanding grinding and lapping, in: The Science of Ceramic Machining and Surface Finishing, vol. II, 1997, pp. 43–60.
[8] A. Carpinteri, B. Chiaia, S. Invernizzi, Numerical analysis of indentation fracture in quasi-brittle materials, Eng. Fract. Mech., in press.
[9] D.E. Miller, Rock drilling with impregnated diamond microbits, Ph.D. Thesis, University of Cape Town, 1986.
[10] M. Borri-Brunetto, B. Chiaia, S. Invernizzi, in: C.A. Brebbia, A. Carpinteri (Eds.), Lacunar Fractality of the Contact Domain in a Closed Rock Fracture, Damage and Fracture Mechanics, CMP, 1998, pp. 545–554.
[11] J. Paone, W.E. Bruce, Drillability Studies—Diamond Drilling, USBM-RI 6324, 1963.
[12] M. Borri-Brunetto, A. Carpinteri, B. Chiaia, Scaling phenomena due to fractal contact in concrete and rock fractures, Int. J. Fract. 95 (1999) 221–238.
[13] C.G. Scott, S. Danyluk, Examination of silicon wear debris generated in a linear scratch test, Wear 152 (1992) 183–185.